

Theory of pure dephasing and the resulting absorption line shape in semiconductor quantum dots

B. Krummheuer, V. M. Axt, and T. Kuhn

Institut für Festkörperteorie, Westfälische Wilhelms-Universität, Wilhelm-Klemm-Str. 10, D-48149 Münster, Germany

(Received 24 August 2001; revised manuscript received 11 December 2001; published 2 May 2002)

The pure dephasing of the optical polarization and the corresponding line shape of absorption spectra in small quantum dots due to the interaction of the exciton both with optical and acoustic phonons is calculated. By restricting ourselves to the exciton ground state we obtain a model which is known to be exactly solvable. We study the temperature dependence and the influence of a static electric field. The spectra exhibit strongly non-Lorentzian line shapes including a sharp zero-phonon line. Optical phonons lead to phonon sidebands which may acquire a finite width due to the dispersion of the phonon branch; the width increases with decreasing dot size. Acoustic phonons both due to deformation potential and piezoelectric coupling lead to a broad background in the spectra which is strongly temperature dependent. Typical features of the spectra are qualitatively well reproduced by a perturbative approach based on one-phonon processes. Multiphonon processes, however, give significant contributions in particular in the case of acoustic phonons. Lateral or vertical electric fields lead to an increasing efficiency of the polar interaction mechanisms while deformation potential interaction is much less influenced.

DOI: 10.1103/PhysRevB.65.195313

PACS number(s): 73.21.La, 78.40.Fy, 63.20.Kr

I. INTRODUCTION

The optical excitation of a semiconductor quantum dot structure, like any other semiconductor structure, with a short coherent light pulse results in the creation of a coherent superposition of valence- and conduction-band states. Subsequently, this phase coherence decays due to various interaction mechanisms of electrons and holes. For many applications such as optoelectronic devices (see, e.g., Ref. 1) a good knowledge of the dephasing is of utmost importance. This holds most prominently if semiconductor quantum dots are to be used as basic building blocks for quantum information processing²⁻⁸ where the operation completely relies on the presence of coherence.

In systems of higher dimensionality like bulk semiconductors or quantum wells the dephasing is typically mainly associated with transitions between different states, i.e., with thermalization, energy relaxation, or recombination processes. These processes require at least approximately the conservation of energy between initial and final state which, in the case of a continuous electronic spectrum, usually can be easily satisfied. In quantum dots, however, the electronic spectrum is discrete and this condition is much harder to fulfill. For the case of carrier-phonon interaction this has resulted in the prediction of a *phonon bottleneck* in the relaxation.^{9,10} The dephasing of optical transitions, on the other hand, is not restricted to such real transitions; instead it is well known¹¹ that also virtual transitions which do not lead to a change of occupations contribute to the dephasing. This contribution is customarily called *pure dephasing*. Due to the large separation between energy levels and the resulting strong reduction of real phonon-mediated transitions between these states it is of particular importance in small quantum dots at elevated temperatures where it dominates with respect to the recombination process.^{12,13}

Quantum dots behave in many aspects similar to atoms with a spectrum which can to a large extent be designed artificially. This fact, together with the ability of integration,

makes them very attractive for applications in quantum information theory. The main difference compared to atoms, however, is the coupling of the electronic degrees of freedom to the lattice which typically results in much faster decoherence times. Experimentally, typical dephasing times of single quantum dots have been found to be in the range from a few tens of picoseconds¹⁴⁻¹⁶ at low temperatures down to several hundreds of femtoseconds¹⁷ at room temperature. By means of four-wave-mixing spectroscopy on an ensemble of dots even dephasing times of more than 600 ps at 7 K have been observed recently.¹⁸ With respect to this behavior quantum dots are more similar to *F* centers in solids which have been investigated over several decades.^{19,20} Therefore it is not surprising that many approaches that have been used in recent years for the theoretical study of dephasing in quantum dots^{12,21,22} are based on models introduced in that context.

In this contribution we present a comprehensive analysis of pure dephasing and the corresponding line shape of absorption spectra due to the interaction with different phonon modes (acoustic and optical) and by different mechanisms (deformation potential, piezoelectric, polar optical) which will be treated both separately and in combination. By comparing the exact results with those obtained by a perturbative treatment of carrier-phonon interaction we clearly identify the role of multiphonon processes. In particular we will address the role of a static electric field both in vertical and lateral direction for the dephasing. Due to the electric field the exciton may acquire a finite dipole moment; the resulting dipole field then induces level shifts in a neighboring dot and thus leads to an effective coupling of different quantum dots. This phenomenon has recently become of great interest since it allows for a conditional coherent dynamics and different implementations based on vertical² or lateral⁸ fields have been proposed to realize basic quantum gates.

Several aspects of pure dephasing in quantum dots have been studied in the past. Schmitt-Rink *et al.*²¹ have extended the theory from *F* centers^{19,20} to semiconductor quantum dots. They give a general formula for the spectrum but they

do not provide numerical results. Takagahara^{12,23} has extracted dephasing times due to the coupling with acoustic phonons. In his perturbative calculations he has included exciton ground and excited states and he has determined the total dephasing rate semiempirically by combining his results with measured population decay rates. He finds a good agreement of the total dephasing rates with experimental data. However, he does not analyze in detail the line shape associated with the coupling to phonons. Uskov *et al.*²² have recently analyzed the dephasing due to the interaction with optical phonons based on an effective coupling which is quadratic in the phonon amplitudes and therefore differs from the usual linear coupling mechanisms. With this mechanism they find a broadening of the zero-phonon line (ZPL) which is not present in the linear coupling model.

The aim of our work is a systematic analysis of the absorption line shape due to carrier-phonon interaction which in general turns out to deviate strongly from a Lorentzian and which exhibits characteristic features for the different interaction mechanisms. We show that in small quantum dots the dispersion of optical phonons comes into play and results in a dephasing of phonon quantum beats. By comparing exact results with approximate treatments we can clearly identify the role of multiphonon processes for the spectral line shape. Finally we analyze how the dynamics of the optical polarization is modified by an applied electric field which is known to strongly influence in particular the polar coupling mechanisms.²⁴

The paper is organized as follows. In Sec. II we briefly introduce the model and the various interaction types and we give both the exact formula for the spectrum as well as the result which is obtained by performing a correlation expansion up to second order in the matrix element. The dynamics of the optically induced polarization as well as the corresponding absorption spectra are presented in Sec. III where we discuss in detail the role of optical- and acoustic-phonon interactions, deviations in the perturbative approach, and the effect of an external field on the dynamics of the polarization. Finally, in Sec. IV we summarize our results.

II. THEORY

A. Model

We consider a model of a quantum dot with well separated sublevels. We are interested in optical transitions from the uppermost level in the valence band to the lowest conduction-band state. The corresponding electronic degrees of freedom shall be represented by Fermi operators c^\dagger , c (d^\dagger , d) for the creation and annihilation of an electron (hole) in the lowest (uppermost) conduction- (valence-) band state. Apart from the dipole coupling to an external laser field our model comprises interactions of the electron and hole with acoustic and optical phonons. More specifically, our model is defined by the following Hamiltonian:

$$H = \hbar\Omega c^\dagger c - \mathbf{M}_0 \cdot \mathbf{E} (c^\dagger d^\dagger + dc) + \hbar \sum_{j,\mathbf{q}} \omega_j(\mathbf{q}) b_{j,\mathbf{q}}^\dagger b_{j,\mathbf{q}} + \hbar \sum_{j,\mathbf{q}} (g_{j,\mathbf{q}}^e b_{j,\mathbf{q}} c^\dagger c - g_{j,\mathbf{q}}^h b_{j,\mathbf{q}} d^\dagger d + \text{H.c.}), \quad (1)$$

where $b_{j,\mathbf{q}}^\dagger$, $b_{j,\mathbf{q}}$ denote Bose operators for the creation and destruction of a phonon in the phonon branch j with wave vector \mathbf{q} and energy $\hbar\omega_j(\mathbf{q})$. The branch index j can represent either longitudinal-optical (LO) phonons, longitudinal-acoustic (LA) phonons, or transverse-acoustic (TA) phonons. It could also refer to interface or confined phonons. Here, however, we will restrict ourselves to the case of bulk phonon modes. $\hbar\Omega$ is the energy of the optical gap including the exciton binding energy but without polaronic renormalizations; note that we have chosen the energy of the hole to define the zero of energy. If the exciton binding energy is smaller than the separation of the single-particle energies the mixing of different states by the Coulomb interaction can be neglected and the excitonic effect reduces to a lowering of the gap by an amount given by the electron-hole Coulomb matrix element.²¹ Finally, \mathbf{M}_0 provides for the dipole coupling to the laser field \mathbf{E} and $g_{j,\mathbf{q}}^{e/h}$ are the phonon coupling matrix elements for the electron and hole, respectively.

Without the dipole coupling the above model is known as the *independent boson model*.²⁵ It has been well known for a long time that independent boson models allow for analytical results. In early studies the phonon-broadened density of electronic states has been calculated for different types of impurities.²⁰ More recently, there was a renewed interest in this model mainly because of its ability to capture essential features of experiments devoted to the coherent control of phonon-quantum beats.^{26–29} It is not too surprising that few-level systems provide for adequate models for zero dimensional structures such as quantum dots, but it turns out that a two-level model coupled to a single LO phonon mode is helpful even for the interpretation of experiments controlling phonon beats in bulk semiconductors.^{26,28} In order to enable a meaningful comparison in the latter case the two levels are identified with the semiconductor ground state and the 1s exciton, respectively.

The goal of the present paper is to analyze the dephasing properties of the optical polarization induced by the phonon coupling defined in Eq. (1). It should be noted that the carrier-phonon interaction in Eq. (1) does not lead to a change of the occupations of the electron or the hole level, because the interaction Hamiltonian commutes with the operators $c^\dagger c$ and $d^\dagger d$ for the respective occupations. The model does therefore not provide for an energy relaxation mechanism. Nevertheless, the phonon coupling may still contribute to the dephasing of the polarization which in this case is called pure dephasing.¹¹ In recent experiments evidence has been found that pure dephasing may become the dominant dephasing mechanism at not too low temperatures for optically excited quantum wells³⁰ or quantum dots.¹³ Furthermore, it was shown in Ref. 12 that the contribution to pure dephasing due to couplings to higher excited states is under realistic conditions considerably smaller than the direct diagonal coupling even in dots which are somewhat larger than those studied here. This finding also justifies our restriction to only two sublevels.

In order to proceed we still have to specify the phonon coupling matrix elements $g_{j,\mathbf{q}}^{e/h}$ for each interaction mechanism relevant for the respective phonon branches. Assuming that the dot and the surrounding barrier material do not differ

significantly in their lattice and dielectric properties we can approximate the phonon modes with the corresponding three-dimensional bulk modes. Then, the coupling matrix elements $g_{j,\mathbf{q}}^{e/h}$ for the electron and hole separate into two factors, where the first depends on the specific coupling mechanism, whereas the second can be calculated from the wave functions $\Psi^{e/h}(\mathbf{r})$ of the electron and hole within the quantum dot potential:

$$g_{j,\mathbf{q}}^{e/h} = \mathcal{G}_{j,\mathbf{q}}^{e/h} \mathcal{F}_{\mathbf{q}}^{e/h}, \quad (2)$$

with the form factors

$$\mathcal{F}_{\mathbf{q}}^{e/h} = \int d^3r |\Psi^{e/h}(\mathbf{r})|^2 e^{i\mathbf{q}\cdot\mathbf{r}}, \quad (3)$$

and $\mathcal{G}_{j,\mathbf{q}}^{e/h}$ is the bulk coupling matrix element.

In this paper we consider the respective influences of three types of carrier-phonon coupling mechanisms: the polar optical coupling to LO phonons, the deformation potential coupling to LA phonons, and the piezoelectric coupling to LA and TA phonons. The polar optical interaction is accounted for by the usual Fröhlich-coupling:

$$\mathcal{G}_{\text{LO},\mathbf{q}}^{e/h} = i \left[\frac{2\pi e^2 \omega_{\text{LO}}(q)}{\hbar 4\pi \epsilon_0 V} \left(\frac{1}{\epsilon_\infty} - \frac{1}{\epsilon_s} \right) \right]^{1/2} \frac{1}{q}, \quad (4)$$

where $q := |\mathbf{q}|$ is the modulus of \mathbf{q} , ϵ_s and ϵ_∞ are the static and high-frequency dielectric constants, respectively, ϵ_0 denotes the vacuum susceptibility, while e represents the elementary charge, and V is a normalization volume. Finally, $\omega_{\text{LO}}(q)$ is the dispersion relation of the LO phonons.

The coupling to acoustic phonons may be mediated either by the deformation potential or via the piezoelectric coupling. While the deformation potential primarily yields interactions with LA phonons, the piezoelectric scattering couples the electronic system to both LA and TA phonons; usually the TA piezoelectric scattering is considerably larger due to the smaller sound velocity.³¹ Accounting together for piezoelectric and deformation potential interactions the coupling $\mathcal{G}_{\text{AC}}^{e/h}$ to acoustic phonons may be written as^{25,31}

$$\mathcal{G}_{\text{AC},j,\mathbf{q}}^{e/h} = \frac{1}{\sqrt{2\rho\hbar\omega_j(q)V}} [qD_j^{e/h} + iM_j(\hat{\mathbf{q}})], \quad (5)$$

where $\hat{\mathbf{q}}$ is the unit vector in the direction of \mathbf{q} , ρ is the density of the semiconductor material and $D_j^{e/h}$ denotes the deformation potential constants for electrons or holes. Finally, M_j provides for the piezoelectric coupling. The branch index j runs over the longitudinal and the two transverse modes and the constants $D_j^{e/h}$ are nonzero only for the LA mode.

The piezoelectric coupling would in principle lead to an anisotropy^{25,31} that is, however, usually neglected. Instead, an effective isotropic model is constructed that is obtained by averaging over the angles. More specifically, it is only the square of $M(\hat{\mathbf{q}})$ that introduces the anisotropy in our final results as will become evident later. Therefore an angle average over this quantity is required. For a crystal with zincblende structure the averaging yields³¹

$$\frac{1}{4\pi} \int_0^{2\pi} d\varphi \int_0^\pi d\theta \sin(\theta) M_j^2(\hat{\mathbf{q}}) = A_j \left(\frac{2ee_{14}}{\epsilon_s \epsilon_0} \right)^2, \quad (6)$$

where e_{14} is the piezoelectric coefficient and A_j are mode dependent geometrical factors that can be found, e.g., in Ref. 31. It should be noted that taking the square modulus of $\mathcal{G}_{\text{LA},\mathbf{q}}^{e/h}$ does not introduce an interference between deformation potential and piezoelectric scattering, because the former is real while the latter is purely imaginary.

Strictly speaking, all three coupling matrix elements are valid only in the long-wavelength limit because they are derived on the basis of a continuum model for the phonons. However, as will be seen in the next section even in the case of the smallest dots studied here the coupling only extends over a relatively small part of the Brillouin zone where the dispersion relations do not deviate much from the continuum case so that these matrix elements can still be considered to be good approximations.

B. Analytical results

It was already mentioned that within independent Boson models it is possible to derive closed-form analytical expressions for a number of linear or nonlinear signals.^{20,25,27–29} The derivation may be done by a number of different theoretical approaches. For our present purposes we have to determine the complex polarization vector \mathbf{P} to linear order in the laser field. As \mathbf{P} is related to the off-diagonal element $Y := \langle dc \rangle$ of the electronic density matrix by

$$\mathbf{P} = \mathbf{M}_0 Y, \quad (7)$$

we have to calculate the linear response of Y . To this end we found it convenient to follow the generating functions approach that was outlined in Refs. 27 and 28 for a single mode system and in Ref. 32 for the multimode case. Specialized to our present model the generating function method involves the following steps: First one has to set up the Heisenberg equation of motion for the generating function,

$$Y(\{\alpha_{j,\mathbf{q}}, \beta_{j,\mathbf{q}}\}) := \langle dc e^{\sum_{j,\mathbf{q}} \alpha_{j,\mathbf{q}} a_{j,\mathbf{q}}} e^{\sum_{j,\mathbf{q}} \beta_{j,\mathbf{q}} b_{j,\mathbf{q}}} \rangle. \quad (8)$$

Up to linear order in the laser field the resulting equation is closed. It is a first-order partial differential equation that is easily solved along the lines described in Refs. 27, 28, and 32. Finally the polarization is obtained from $\mathbf{P} = \mathbf{M}_0 Y = \mathbf{M}_0 Y(\{\alpha_{j,\mathbf{q}} = \beta_{j,\mathbf{q}} = 0\})$. As a result of this procedure we find in agreement with previous results²¹ that the linear polarization induced by a δ -like laser pulse, i.e., $\mathbf{E}(t) = \mathbf{E}_0 \delta(t)$, which is polarized parallel to \mathbf{M}_0 is given by

$$\mathbf{P}(t) = \Theta(t) \frac{i|\mathbf{M}_0|^2 \mathbf{E}_0}{\hbar} e^{-i\bar{\Omega}t} \exp \left[\sum_{j,\mathbf{q}} |\gamma_{j,\mathbf{q}}|^2 (e^{-i\omega_j(q)t} - n_j(q) |e^{-i\omega_j(q)t} - 1|^2 - 1) \right] =: \epsilon_0 \chi(t) \mathbf{E}_0, \quad (9)$$

where

$$n_j(q) := \frac{1}{e^{\hbar\omega_j(q)/k_bT} - 1} \quad (10)$$

stands for the equilibrium phonon occupation at temperature T , $\gamma_{j,\mathbf{q}} := g_{j,\mathbf{q}}^x / \omega_j(q)$ is a dimensionless coupling strength, $g_{j,\mathbf{q}}^x := g_{j,\mathbf{q}}^e - g_{j,\mathbf{q}}^h$ being the exciton coupling matrix element, and

$$\bar{\Omega} := \Omega - \sum_{j,\mathbf{q}} \omega_j(q) |\gamma_{j,\mathbf{q}}|^2 \quad (11)$$

represents the polaron shifted transition frequency. In the case of optical phonons the quantity $S := \sum_{\mathbf{q}} |\gamma_{\text{LO},\mathbf{q}}|^2$ is usually called the Huang-Rhys parameter.^{19,21} In the derivation of Eq. (9) it has been assumed that before the laser excitation the system is in the electronic ground state and that the statistical operator for the phonon system initially corresponds to an equilibrium distribution at temperature T and is thus given by

$$\hat{\rho}_{\text{ph}} = \frac{e^{-H_{\text{ph}}^0/k_bT}}{\text{Tr}(e^{-H_{\text{ph}}^0/k_bT})}, \quad (12)$$

with $H_{\text{ph}}^0 := \sum_{j,\mathbf{q}} \hbar\omega_j(\mathbf{q}) b_{j,\mathbf{q}}^\dagger b_{j,\mathbf{q}}$. The linear susceptibility $\chi(t)$ defined in Eq. (9) comprises contributions from all possible multiphonon processes. It is valid for arbitrary coupling strengths and temperatures. Using Eq. (9) it is easy to determine the linear absorption spectrum as the absorption coefficient at frequency ω is directly proportional to the imaginary part $\sim \text{Im}[\chi(\omega)]$ where $\chi(\omega)$ is the Fourier transform of $\chi(t)$. In numerically performing the Fourier transform some care has to be taken, as the corresponding spectrum may contain unbroadened lines because energy relaxation is not included in our model. We have obtained our numerical results by multiplying $\chi(t)$ by a factor e^{-t/t_0} and then performing the Fourier transformation. As we are interested in seeing the effect of pure dephasing separately from other dephasing mechanisms we have chosen the rather long time constant of $t_0 = 500$ ps which is longer than typical estimates for real energy relaxation or recombination times.

C. Perturbative approach

For models with more complicated coupling schemes it is usually not possible to obtain analytical results. Mostly perturbative approaches are used in these cases in order to approximate the desired spectrum. It is therefore instructive to compare the analytical result [Eq. (9)] with the outcome of commonly used approximations. A widely used method for quantum kinetic studies of the carrier-phonon interaction is the correlation expansion.^{33,34} Within this approach one starts with the equation of motion for the off-diagonal element Y of the density matrix which reads

$$\frac{\partial}{\partial t} Y = -i\Omega Y + \frac{i}{\hbar} \mathbf{M}_0 \cdot \mathbf{E} - i \sum_{j,\mathbf{q}} [g_{j,\mathbf{q}}^x Y_{j,\mathbf{q}}^{(-)} + g_{j,\mathbf{q}}^{x*} Y_{j,\mathbf{q}}^{(+)}], \quad (13)$$

where the *phonon-assisted* density matrices $Y_{j,\mathbf{q}}^{(-)}$ and $Y_{j,\mathbf{q}}^{(+)}$ are defined as $Y_{j,\mathbf{q}}^{(-)} := \langle dcb_{j,\mathbf{q}} \rangle$ and $Y_{j,\mathbf{q}}^{(+)} := \langle dcb_{j,\mathbf{q}}^\dagger \rangle$. Unlike the equation of motion for the generating function $Y(\{\alpha_{j,\mathbf{q}}, \beta_{j,\mathbf{q}}\})$, Eq. (13) is not closed; instead it is the starting point for an infinite hierarchy of higher-order phonon-assisted density matrices. The idea of the correlation expansion is to truncate the phonon-assisted hierarchy by factorizing higher order phonon-assisted density matrices on a chosen level. Mostly the truncation is invoked after the first step, i.e., one writes down equations of motion for the density matrices $Y_{j,\mathbf{q}}^{(-)}$ and $Y_{j,\mathbf{q}}^{(+)}$ and factorizes the density matrices with double phonon assistances, e.g., according to $\langle dcb_{j,\mathbf{q}}^\dagger b_{j,\mathbf{q}} \rangle \approx \langle dc \rangle \langle b_{j,\mathbf{q}}^\dagger b_{j,\mathbf{q}} \rangle$. This procedure results in the following equations for the phonon-assisted density matrices:

$$\begin{aligned} \frac{\partial}{\partial t} Y_{j,\mathbf{q}}^{(-)} &= -i[\Omega + \omega_j(q)] Y_{j,\mathbf{q}}^{(-)} - i g_{j,\mathbf{q}}^{x*} [1 + n_j(q)] Y, \\ \frac{\partial}{\partial t} Y_{j,\mathbf{q}}^{(+)} &= -i[\Omega - \omega_j(q)] Y_{j,\mathbf{q}}^{(+)} - i g_{j,\mathbf{q}}^x n_j(q) Y. \end{aligned} \quad (14)$$

It is easy to verify that the correlation expansion truncated at this level yields results that are correct up to second order in the phonon coupling. The solution of Eqs. (13) and (14) may be obtained by taking the Fourier transforms of these equations. From the relation between Y and the polarization one can then directly read off the linear susceptibility in frequency space:

$$\begin{aligned} \chi(\omega) &= \frac{|\mathbf{M}_0|^2}{\hbar \epsilon_0} \left[\Omega - \omega - i\gamma_0 + \sum_{j,\mathbf{q}} \frac{|g_{j,\mathbf{q}}^x|^2 [1 + n_j(q)]}{\omega + i\gamma_0 - \Omega - \omega_j(q)} \right. \\ &\quad \left. + \sum_{j,\mathbf{q}} \frac{|g_{j,\mathbf{q}}^x|^2 n_j(q)}{\omega + i\gamma_0 - \Omega + \omega_j(q)} \right]^{-1}. \end{aligned} \quad (15)$$

Here, we have introduced a finite minimal spectral width given by $\gamma_0 = 1/t_0$, which corresponds to the finite decay also used in the Fourier transform of the exact result.

III. RESULTS

We have applied the theory described above to a prototype GaAs quantum dot which is confined in the vertical (z) direction by infinite barriers while in the lateral (x, y) plane a parabolic confinement potential is assumed.³⁵ We take the same potential shape for electrons and holes, this results in a lateral extension of the hole wave function which is by a factor of $(m_e/m_h)^{(1/4)} \approx 0.87$ smaller than the electron wave function. The vertical size of the dot is given by the well width while we defined the lateral size as the radius where the electron density is reduced to half its maximum value.

In order to include the dispersion of the LO phonon branch we have taken the shape of the dispersion relation obtained from a standard diatomic linear chain model adjusted to the phonon dispersion relation given in the literature.³⁶ All phonon branches have been taken as isotropic. The material parameters used in the calculations are summarized in Table I. The dispersion relations of the

TABLE I. Material parameters taken from Ref. 48 except for the deformation potentials which are taken from Ref. 12. The in-plane and vertical effective masses of the holes are calculated from the Luttinger parameters according to the standard formulas; (Ref. 35); m_0 is the free-electron mass.

Effective electron mass m_e	0.067 m_0
Effective hole mass $m_h^{x,y}$ (in plane)	0.112 m_0
Effective hole mass m_h^z (vertical)	0.377 m_0
LO phonon energy $\hbar \omega_{LO}$	36.4 meV
Static dielectric constant ϵ_s	12.53
High-frequency dielectric constant ϵ_∞	10.9
Density ρ	5.37 g/cm ³
Logitudinal sound velocity v_L	5110 m/s
Transverse sound velocity v_T	3340 m/s
Deformation potential for electrons D^e	-14.6 eV
Deformation potential for holes D^h	-4.8 eV
Piezoelectric constant e_{14}	0.16 C/m ²

phonons are shown in Fig. 1 together with the angular integrated effective form factors

$$\mathcal{F}^{\text{eff}}(q) := \int_0^{2\pi} d\varphi \int_0^\pi d\theta \sin(\theta) |\mathcal{F}_q^e - \mathcal{F}_q^h|^2 \quad (16)$$

corresponding to three different dot sizes. In all cases lateral and vertical size have been taken to be equal. In the case of the polar interaction mechanisms this effective form factor directly determines the region in the phonon \mathbf{q} space to which the dot is effectively coupled. For deformation potential interaction due to different deformation potentials of electrons and holes a somewhat different quantity should appear in the integral, but also in this case Eq. (16) provides a good estimate of the range of relevant q values. With decreasing dot size the form factors extend to higher \mathbf{q} values. It is clearly seen that for large dots the assumptions of a constant LO phonon frequency as it is usually applied in systems of higher dimensionality is quite well satisfied while quantum dots below about 10 nm start to feel the dispersion. This means that the combined electron-LO-phonon system

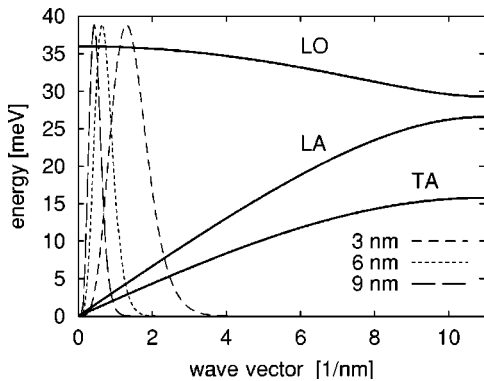


FIG. 1. Dispersion relations of the LO, LA, and TA phonons taken in the calculations as well as normalized effective form factors [see Eq. (16)] describing the coupling of quantum dots with three different sizes to the various phonon modes.

changes from a purely discrete system into one with a continuum part in the spectrum. Also in the case of acoustic phonons the relevant range of phonon frequencies increases with decreasing dot size leading to an effectively increasing width of the continuum in the spectrum. Down to the smallest dots studied here Fig. 1 shows that the assumption of linear dispersion of both longitudinal and transverse acoustic phonons is well satisfied. Nevertheless, for the numerical evaluation of the formulas we have always taken the full dispersion.

A. Dephasing due to optical-phonon interaction

Let us first concentrate on the real time dynamics of the optically induced polarization in the electron-LO-phonon system. If the dispersion of the phonons is neglected it is clearly seen from Eq. (9) that the result is exactly the same as in the case of single phonon mode with the effective interaction matrix element $g_{\text{eff}} = \sqrt{\sum_{\mathbf{q}} |g_{\mathbf{q}}^e - g_{\mathbf{q}}^h|^2}$. This single mode model has been studied in detail also in view of nonlinear optical signals, in particular the coherent control of phonon quantum beats in four-wave mixing signals, and the role of a stronger electron-phonon coupling in Refs. 27–29 and 37. The optical polarization resulting from the excitation with an optical pulse with a δ -function-like shape in time as well as the corresponding absorption spectrum are shown for the case of a 6-nm quantum dot at a temperature of 300 K in Figs. 2(a) and (b). The optical polarization exhibits quantum beats with the phonon frequency; no decay is present. The spectrum consists of a series of δ -function peaks at the zero-phonon transition and at integer multiples of the phonon frequency above and, for nonzero temperature, below that transition. The weights of the various lines depend on temperature and, through the effective coupling constant (or the Huang-Rhys parameter), on the quantum dot parameters. A closed-form analytical expression in terms of Bessel functions can be found in Refs. 19 and 21. Such phonon-assisted optical transitions in quantum dots have been observed in resonant Raman scattering³⁸ as well as in photoluminescence and photoluminescence-excitation spectroscopy.^{24,39}

Without phonon dispersion the spectrum of the electron-phonon system is completely discrete. If the dispersion of the LO phonons is taken into account the system now has continuum parts and therefore decay processes are possible. The resulting optical polarization and the corresponding absorption spectra for the 6-nm dot are plotted in Figs. 2(c) and (d) under the same excitation condition as above while Figs. 2(e) and (f) display the results for a 3-nm dot. We clearly see that the phonon quantum beats in the optical polarization [Figs. 2(c) and (e)] are damped. The typical time scale for this damping is about 50 ps in the case of the 6-nm dot while it is about 10 ps for the 3-nm dot. This strong size dependence can be well understood from Fig. 1 which shows that the form factor of the small dot effectively probes a considerably broader range of frequencies leading to a faster decay due to destructive interference of the various \mathbf{q} components in the polarization. The spectra now consist of the unbroadened ZPL as well as LO phonon sidebands which are broadened according to the frequency range of phonons which effec-

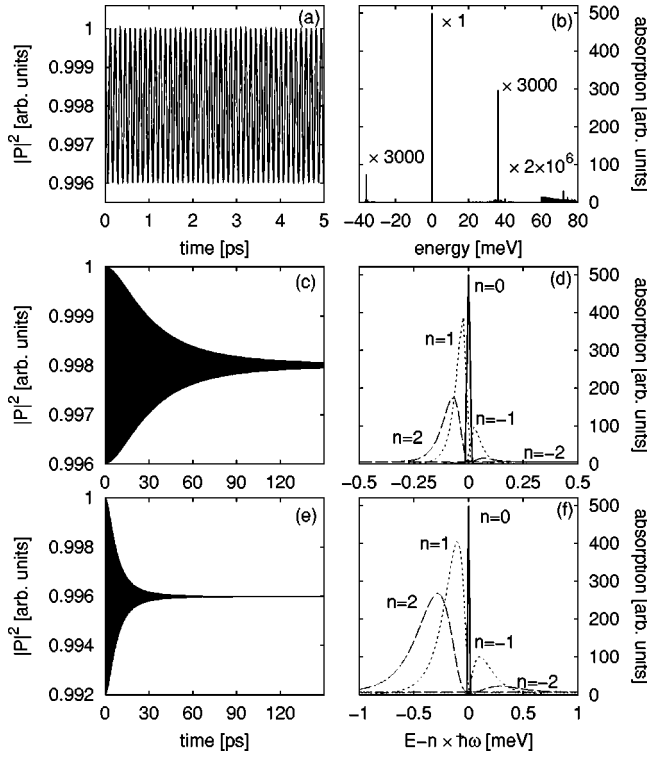


FIG. 2. Optical polarizations induced by a δ -function-shaped optical pulse (left column) and absorption spectra (right column) for a quantum dot interacting with optical phonons at a temperature of 300 K. Parts (a) and (b) refer to a calculation without phonon dispersion, in parts (c) and (d) [(e) and (f)] the results including dispersion are plotted for a 6-nm (3-nm) quantum dot. The spectra of the n -phonon sidebands due to phonon emission ($n > 0$) or phonon absorption ($n < 0$) are shifted by $-n\hbar\omega$ towards the ZPL. In part (d) they are multiplied by the factors 3×10^3 ($|n|=1$) and 2×10^6 ($|n|=2$); the corresponding factors in part (f) are 3×10^4 ($|n|=1$) and 4×10^7 ($|n|=2$).

tively couple to the exciton. For a better comparison in Figs. 2(d) and (f) we have shifted the $|n|$ -phonon emission or absorption sideband towards the ZPL by subtracting or adding $n\hbar\omega_{LO}(0)$ and they have been multiplied by the respective factors given in the caption. Here, $n > 0$ refers to emission and $n < 0$ to absorption sidebands. Since $\omega_{LO}(0)$ is the maximum frequency of the LO phonons the emission sidebands are now completely below the ZPL while the absorption sidebands are above this line. It is clearly seen that the $|n|=2$ sidebands, corresponding to two-phonon transitions, exhibit a width which is twice the width of the $|n|=1$ sidebands. Furthermore, the widths in the case of the 3-nm dot are approximately a factor of 5 larger than for the 6-nm dot corresponding to the enhanced damping of the quantum beats discussed above. We want to remark that the small but nonzero width of the ZPL is due to the additional phenomenological dephasing time $t_0 = 500$ ps which has been introduced to perform the Fourier transformation.

B. Dephasing due to acoustic-phonon interaction

Acoustic phonons are characterized by a continuous spectrum starting at zero frequency. Therefore the phonon side-

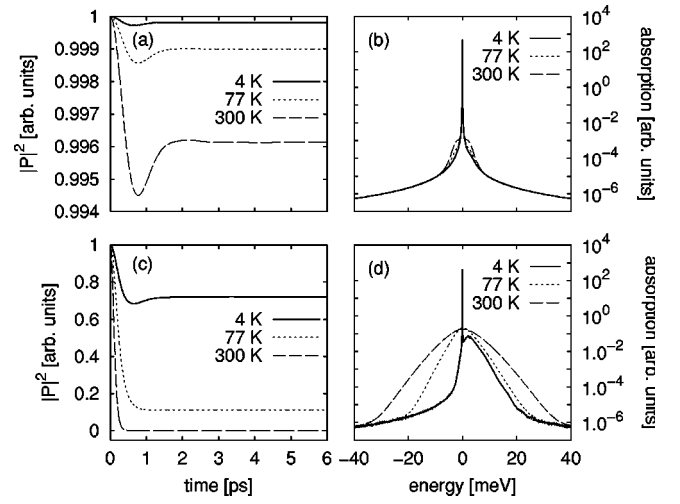


FIG. 3. Optical polarizations induced by a δ -function-shaped optical pulse (left column) and absorption spectra (right column) for a 3-nm quantum dot interacting with acoustic phonons at three different temperatures. Parts (a) and (b) refer to piezoelectric coupling, parts (c) and (d) to deformation potential coupling.

bands approach the ZPL and, under suitable conditions, may result in a broadened ZPL.²⁰ In Fig. 3 we have plotted the optical polarization and the absorption spectrum for a 3-nm quantum dot at three different temperatures as obtained from calculations including piezoelectric [Figs. 3(a) and (b)] and deformation potential [Figs. 3(c) and (d)] coupling. Interestingly, we find that in all cases the polarization remains at a finite value at long times corresponding to an unbroadened ZPL. This can be understood from the \mathbf{q} dependence of the matrix element in the limit of small \mathbf{q} values. According to Eq. (5) the bulk coupling matrix elements of deformation and piezoelectric coupling are proportional to \sqrt{q} and $1/\sqrt{q}$, respectively. The deformation potential for electrons and holes are, in general, different, and the form factors of both carrier types approach unity for $q \rightarrow 0$, therefore the total coupling constant is proportional to \sqrt{q} . The bulk piezoelectric coupling constant, on the other hand, being a polar mechanism, has exactly the same value for electrons and holes. Then, the form factors of the electron and hole exactly cancel at $q=0$. The lowest order the in difference of the form factors is proportional to q^2 and thus the total coupling constant is proportional to $q^{3/2}$. A vanishing coupling constant for $q \rightarrow 0$ gives rise to an unbroadened ZPL (see the Appendix for a more detailed discussion). This is in contrast to the electron spectral function which has been calculated already in 1965 by Duke and Mahan²⁰ for the case of impurity spectra. Since in their case there is no cancellation between the electron and hole part they find a broadening of the ZPL for piezoelectric coupling while deformation potential results in a sharp ZPL.

As can be expected the dynamics due to interactions with acoustic phonons exhibits a pronounced temperature dependence. At low temperatures the line is strongly asymmetric; there is only a contribution on the high-energy side of the ZPL due to phonon emission. With increasing temperature phonon absorption processes come into play and the line

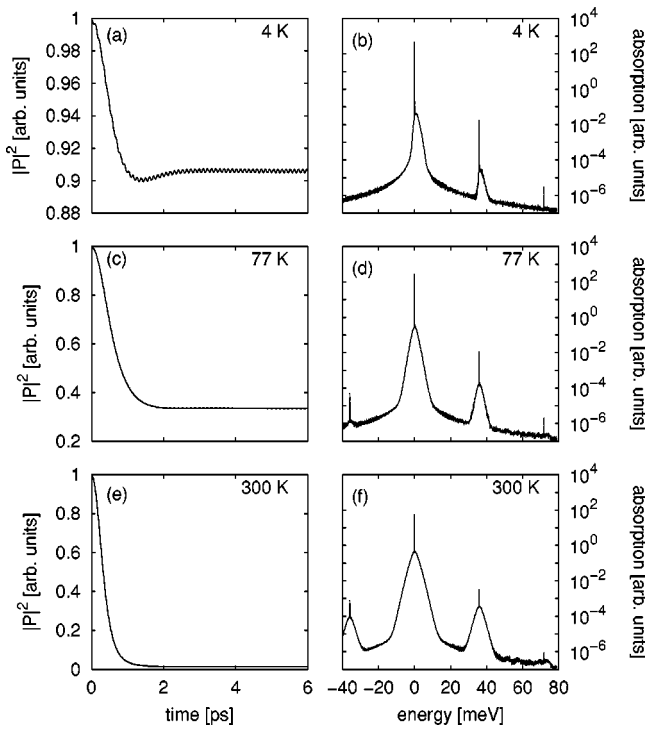


FIG. 4. Optical polarizations induced by a δ -function-like optical pulse (left column) and absorption spectra (right column) for a 6-nm quantum dot interacting with optical and acoustic phonons at three different temperatures.

becomes more symmetric. Furthermore, the weight of the ZPL is reduced resulting in lower long time values of the polarization. By comparing the results for deformation potential and piezoelectric coupling we find, in agreement with Takagahara,¹² that the deformation potential contribution is clearly dominant. Even at 300 K piezoelectric coupling reduces the initial coherence by less than one percent. This is due to the large electron-hole overlap which strongly reduces all polar interaction mechanisms. We will come back to this point below when discussing the influence of an electric field.

C. Combined dynamics

Let us now combine the results of the previous sections by taking into account simultaneously all three types of interaction mechanisms. Figure 4 shows the optical polarizations and the corresponding absorption spectra at three different temperatures for the case of a 6-nm quantum dot. The overall dynamics of the polarization is dominated by deformation potential interaction. Superimposed there are quantum beats due to LO phonon coupling which, due to the different scales of the polarization axes, are visible only at the lowest temperature. Around the ZPL we see the lineshape due to acoustic-phonon interaction as discussed in the previous section. This line is then repeated, however, with decreasing strength, at multiples of the LO phonon frequency. Thus each LO phonon sideband acquires a background due to acoustic-phonon interaction. Very similar spectra consisting of a narrow ZPL and a broad background have recently been ob-

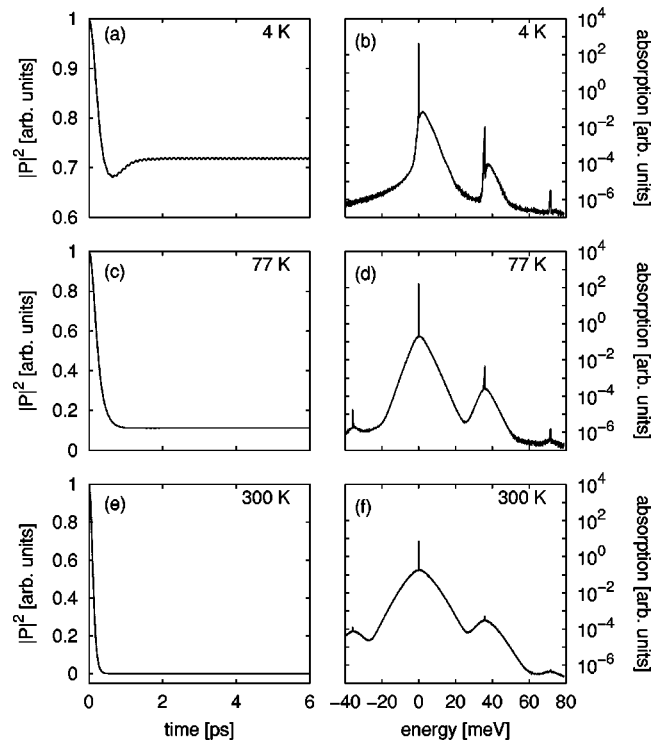


FIG. 5. Same as Fig. 4 but for a 3-nm quantum dot.

served in four-wave-mixing experiments on InGaAs quantum dots.¹⁸ Even if these spectra do not exactly coincide with the linear absorption spectra as calculated here, they are strongly related because time-integrated four-wave-mixing signals at least in few-level systems essentially measure the linear polarization dynamics.

In Fig. 5 the polarization curves and absorption spectra at the same temperatures as above are plotted for a quantum dot of 3 nm size. The extension of the form factor to larger q values results in a pronounced increase in the widths of the acoustic-phonon contribution in the spectra and a substantially faster initial decay of the polarization which now occurs on a time scale of 100 fs. In particular at 300 K the acoustic wings of the different LO phonon sidebands now merge and result in a smooth spectrum up to high energies.

D. Comparison with the perturbative approach

A particular feature of the independent boson model used here is the fact that it can be solved analytically. This feature is typically lost if the model is extended, e.g., by taking into account excited exciton states and phonon-induced transitions between these states. In such cases approximate techniques have to be used. The present model provides the opportunity to compare the exact results with results obtained from a correlation expansion as it is often applied in more complex and higher dimensional systems and therefore it allows us to clearly analyze the deviations between exact and approximate solutions, which in most other cases is not possible.

In Fig. 6 we compare the absorption spectra of a 3-nm quantum dot obtained from the exact solution (left column)

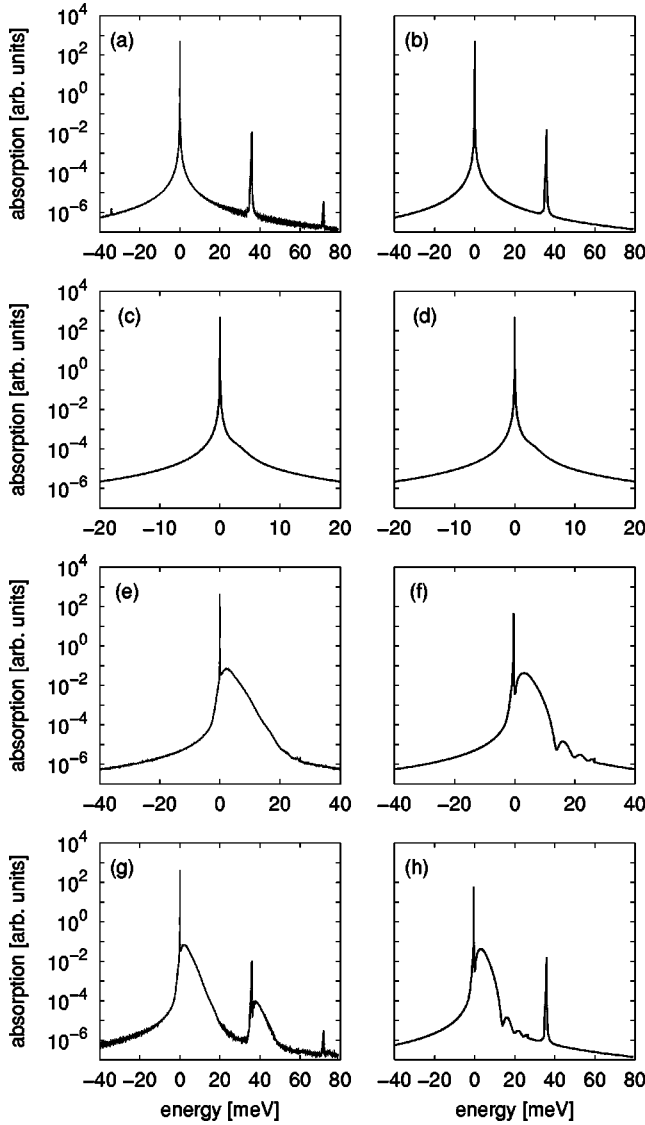


FIG. 6. Comparison of the exact absorption spectra (left column) with those obtained from a correlation expansion up to the second order in the coupling matrix elements (right column) for polar optical [(a) and (b)], piezoelectric [(c) and (d)], and deformation potential [(e) and (f)], as well as for the combination of all mechanisms [(g) and (h)] at a temperature of 4 K.

with the spectra obtained from the correlation expansion up to second order in the interaction matrix element [Eq. (15)] at a temperature of 4 K for the individual interaction mechanisms as well as for the complete model. In the case of the polar optical interaction [Figs. 6(a) and (b)] we find a good agreement for the ZPL and for the first phonon sideband. Of course, the second sideband, involving a two-phonon transition, is absent in the perturbative result because multiphonon processes are neglected on this level. As has been shown in the previous sections the piezoelectric interaction is very weak. In particular at low temperatures it gives only a very small contribution to the spectrum. Therefore it is not surprising that multiphonon processes are negligible and exact and perturbative results are in good agreement [Figs. 6(c) and (d)]. In the case of deformation potential coupling [Figs.

6(e) and (f)] we find that when comparing exact and approximate solutions both the height and the width of the spectrum are in quite good agreement. However, there are remarkable differences in the detailed shape. First, in the perturbative result the dip above the ZPL is much more pronounced than in the exact result. This is due to the fact that one-phonon transitions with a small wave vector are strongly suppressed because, as already discussed above, in this range the matrix element is proportional to \sqrt{q} . Therefore positions in the immediate vicinity of the ZPL can only be reached by at least two-phonon processes which again are absent in the perturbative treatment. Second, the approximate absorption spectrum exhibits a series of dips above 10 meV which is absent in the exact result. These dips result from the form factor, in particular from the Fourier transform of the cosine wave function in the z direction. We have checked that they are absent if also in this direction a Gaussian wave function is used. In the exact result these dips are obviously washed out due to multiphonon processes. Third, the approximate spectrum exhibits a sharp cutoff at an energy of 26 meV corresponding to the maximum energy of LA phonons (see Fig. 1) because higher energies are not accessible in a one-phonon process. Finally, in Figs. 6(g) and (h) the spectra of the full model are compared. Besides the features already discussed the most pronounced difference is the missing acoustic background of the one-LO phonon sideband. Of course, this background involves at least one optical and one acoustic phonon and it is therefore at least related to two-phonon processes and thus it is absent in the perturbative treatment which takes into account only one-phonon processes.

E. Influence of a static electric field

Polar interaction mechanisms are completely absent if the system is locally electrically neutral, i.e., if the electron and hole wave functions are identical. In the cases studied so far the wave functions were slightly different because of the different confinement of electron and hole in the lateral directions due to the different masses. If an electric field is applied to such a structure, the electron and hole wave functions are displaced with respect to each other. Then, the q dependence of the difference between electron and hole form factors in the range of small q values changes from quadratic to linear resulting in an increasing polar coupling efficiency.²⁴ Such an electric field can be applied in the vertical or in the lateral direction. In this section we will study the influence of an electric field in these two directions on the dynamics of the optical polarization.

A vertical electric field gives rise to the quantum confined Stark effect.^{40–43} Electron and hole are separated towards the opposite edges of the confining quantum well potential. Such an electric field may be applied externally, but in materials like GaN it may exist even intrinsically due to polarization charges.⁴⁴ Furthermore, by applying a vertical electric field we can model the situation which is present in many pyramidal quantum dot structures that the wave function of one carrier type is located more towards the base of the pyramid while the other is located close to the top.^{42,45–47} The application of a lateral electric field, on the other hand, has re-

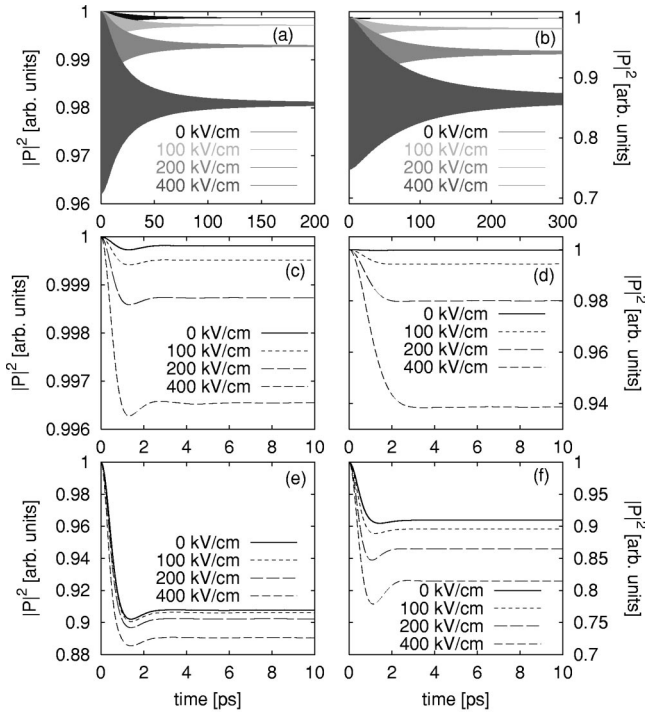


FIG. 7. Optical polarizations induced by a δ -function-shaped optical pulse for a 6-nm quantum dot interacting with phonons via polar optical [(a) and (b)], piezoelectric [(c) and (d)], and deformation potential [(e) and (f)] interaction in the presence of a static vertical (left column) and lateral (right column) electric field at a temperature of 4 K.

cently become of interest because it has been shown that in this case the different dipole moments associated with the ground and excited states of the dot, respectively, may be used to couple different quantum dots and to perform a conditional dynamics which serves as a basic building block for quantum information processing.⁸ The same type of dipole coupling has been proposed for the case of vertical fields.² However, since in that proposal a dynamics based on transitions between different conduction-band levels has been used it does not directly fit our model.

Figure 7 shows the temporal evolution of the optical polarization after excitation with a δ -shaped pulse at a temperature of 4 K for the case of a vertical (left column) and lateral (right column) electric field of different strengths. In the case of polar optical interaction [Figs. 7(a) and (b)] we clearly see that with increasing field strength the initial amplitude of the phonon quantum beats considerably increases and the long-time value of the polarization decreases. This is because with increasing coupling efficiency the relative weight of the phonon sideband is enhanced leading to a more pronounced beating and a smaller weight of the ZPL which determines the final value of the polarization. At a given field value this effect is much stronger for a lateral field than for a vertical field because in the vertical case the separation of electron and hole wave function is limited by the width of the confining potential well while in the lateral direction no such limitation exists. Furthermore, we notice that the time scale of the initial decay in the vertical case is essentially not af-

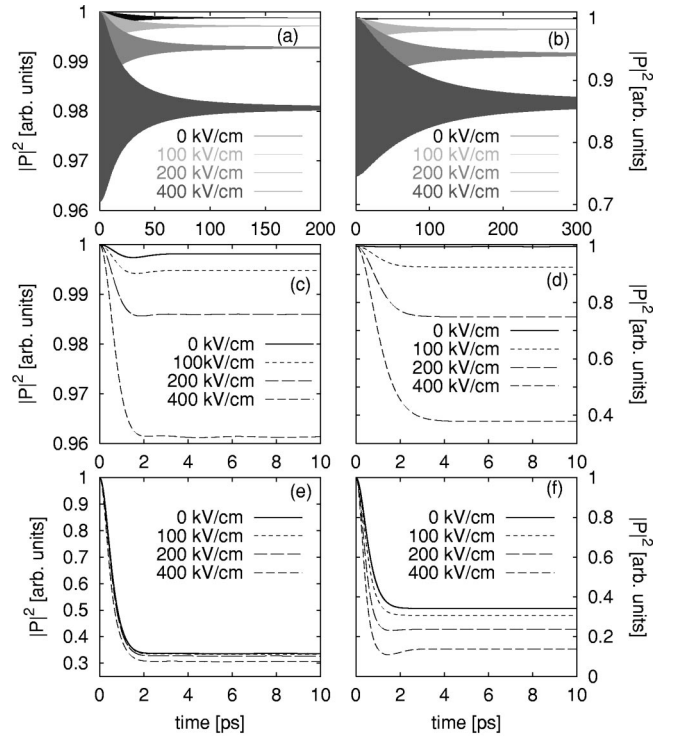


FIG. 8. Same as Fig. 7 but at a temperature of 77 K.

ected while in the lateral case the decay time of the beats is increased by a factor of about 3. This is again a result of the width of the effective form factor in q space which is reduced when the electron-hole overlap is reduced.

The piezoelectric interaction [Figs. 7(c) and (d)], being also a polar interaction mechanism, exhibits essentially the same behavior as the polar optical case. It is also strongly enhanced by electric fields. Notice that while without field the initial coherence is reduced only by a factor of about 2×10^{-4} at a field of 400 kV/cm this reduction is enhanced to a factor of 3.5×10^{-3} for a vertical and even 6×10^{-2} for a lateral field.

The deformation potential interaction [Figs. 7(e) and (f)] is much less affected by the field because in this case, due to different deformation potentials of electrons and holes, there is no cancellation of electron and hole form factors at zero electric field. Nevertheless, there is a slight enhancement of the dephasing efficiency with increasing field. In contrast to the polar mechanisms, here the time scale of the initial decay is not affected by the field. Due to the absence of cancellation effects the extension of the effective form factor in momentum space is here always directly determined by the spatial extension of electron and hole wave function. In a parabolic confinement potential, as is assumed here in the lateral direction, a static field leads only to a rigid displacement of electron and hole wave functions without changing their respective shapes. In a vertical field the shape of the wave functions is modified, however, in the fields considered here the spatial widths do not change much. Therefore the extension of the form factor in momentum space only slightly depends on the field.

In Fig. 8 the same polarization curves for vertical and

lateral fields are plotted at a temperature of 77 K. For polar optical interaction the results are essentially the same because 77 K is still much less than the temperature of 422 K corresponding to $\hbar\omega_{LO}(0)$. The acoustic interaction mechanisms, on the other hand, are strongly enhanced compared to the 4-K case. In the presence of a lateral field of 400 kV/cm piezoelectric interaction now results in a reduction of the initial coherence of the order of 60% and it is therefore of the same order of magnitude as the deformation potential interaction which gives rise to a reduction of about 85%. Therefore in the presence of strong electric fields there may be situations where the dephasing due to the piezoelectric interaction is no more negligible compared to the deformation potential interaction.

IV. CONCLUSIONS

We have presented a detailed analysis of the loss of interband coherence due to carrier-phonon interaction in an optically excited quantum dot. Only the ground-state exciton has been taken into account, therefore we have restricted ourselves to the case of small quantum dots where the excited states are sufficiently far above the ground state. In this case it has indeed been shown that the dominant contribution to the dephasing stems from the ground state and excited states give rise to a minor correction.¹² The main advantage of the present model is the fact that it can be solved exactly and thus multiphonon processes of all orders involving equal as well as different types of phonons are fully included. Besides being a relevant model for small quantum dots it is therefore an ideal test case to study the validity of approximate techniques.

The general finding is that none of the coupling mechanisms studied, polar optical, piezoelectric, and deformation potential interaction, results in an exponential decay or, equivalently, in a Lorentzian line shape characterized by a single decay time. In all cases the optically induced polarization exhibits an initial decay on a time scale which is essentially determined by the range of phonon frequency accessible by the interaction matrix element. This range is mainly determined by the form factor resulting from the electron and hole wave functions. This frequency range increases with decreasing dot size leading to a faster initial decay. However, even this initial decay is in general strongly nonexponential. After this initial decay the polarization retains a finite value corresponding to a sharp ZPL in the spectrum. The level of this remaining polarization or, equivalently, the weight of the ZPL in the spectrum strongly depends on the interaction mechanism and on the temperature. For high temperatures essentially all of the polarization is destroyed. This is in line with recent studies where pure dephasing has been found to be the dominant decoherence mechanism at elevated temperature.¹³ Piezoelectric coupling turns out to be insignificant in most cases and at elevated temperatures deformation potential interaction is the most important process for the loss of coherence. It should be noted that the non-Lorentzian line shape of the spectra has interesting consequences for the more realistic case of excitation with pulses of finite duration. All the polarization curves shown here

have been calculated for an excitation with a δ -function-shaped pulse which excites all frequency components with the same weight. Of course, a pulse with a finite width excites only a part of the spectrum. Therefore in the case of resonant excitation the weight of the ZPL in the excited polarization may be considerably enhanced resulting in a considerably higher value of the long-time coherence than in the curves presented here.

When comparing the exact results with a perturbative treatment we find that in the present case of a GaAs quantum dot, where all phonon couplings are relatively weak, both the height and the width of phonon-related structures in the spectra are in quite good agreement. The perturbative approach, however, may produce some sharp spectral features related to details in the matrix elements, in particular if some frequencies are not accessible by one-phonon transitions. These features are much less pronounced or even completely smoothed out in the exact result. Therefore some care should be taken when such structures appear in perturbative calculations of more complex systems where a comparison with the exact solution is not possible.

Finally we have shown that a static electric field, both in the vertical and the lateral direction, has a pronounced effect on the dephasing, in particular the dephasing due to the polar interaction mechanisms. By displacing the electron and hole wave functions with respect to each other the polar matrix elements are strongly enhanced. This reduces the remaining coherence, i.e., the weight of the ZPL in the spectrum. The initial decay or, in the case of polar optical interaction, the decay of the phonon quantum beats, is slowed down by strong lateral fields because the range of accessible phonon frequencies determined by the effective form factor is reduced. Deformation potential interaction, on the other hand, is much less influenced by the electric field. Thus in very high fields piezoelectric and deformation potential interaction may even become of comparable strength. In addition to the modification of the pure dephasing processes discussed in this paper such electric fields will also modify the radiative recombination. Due to the reduced electron-hole overlap the dipole matrix element will be reduced resulting in an increasing T_1 time. Thus the relative contribution of pure dephasing to the total dephasing may be enhanced.

ACKNOWLEDGMENTS

This work has been supported by the European Commission within the FET project IST-1999-11311 (Semiconductor-based Implementation of Quantum Information Devices) as well as by the Deutsche Forschungsgemeinschaft (DFG) in the framework of the Schwerpunktprogramm Quantenkohärenz in Halbleitern. V.M.A. acknowledges financial support of the DFG through a Habilitationstipendium.

APPENDIX: ASYMPTOTICS OF THE POLARIZATION FOR LONG TIMES

The purpose of this Appendix is to discuss the asymptotic behavior of the linear polarization in the limit of $t \rightarrow \infty$. In

particular we want to show explicitly that the polarization does not vanish in this limit, reflecting the fact that the zero-phonon line is unbroadened in our model.

According to Eq. (9) the absolute modulus of the polarization is given by

$$|\mathbf{P}(t)| = \Theta(t) \frac{|\mathbf{M}_0|^2 |\mathbf{E}_0|}{\hbar} \exp[-F(t)], \quad (\text{A1})$$

where

$$\begin{aligned} F(t) &= \sum_{j,\mathbf{q}} |\gamma_{j,\mathbf{q}}|^2 \text{Re}(1 - e^{-i\omega_j(q)t} + n_j(q) |e^{-i\omega_j(q)t} - 1|^2) \\ &= \sum_j \int_0^{Q_B} dq q^2 \Gamma_j(q) [2 + 4n_j(q)] \sin^2\left(\frac{\omega_j(q)}{2} t\right), \end{aligned} \quad (\text{A2})$$

with

$$\Gamma_j(q) = \int_0^{2\pi} d\varphi \int_0^\pi d\theta \sin(\theta) \frac{V}{(2\pi)^3} |\gamma_{j,\mathbf{q}}|^2. \quad (\text{A3})$$

In Eq. (A2) we have converted the sum over \mathbf{q} into an integration, where Q_B marks the boundary of the Brillouin zone. Obviously, a vanishing $|P(t)|$ for long times is equivalent to the requirement that the function $F(t)$ approaches infinity for $t \rightarrow \infty$. However, the integral (A2) can easily be estimated as follows:

$$\begin{aligned} 0 &\leq \int_0^{Q_B} dq q^2 \Gamma_j(q) [2 + 4n_j(q)] \sin^2\left(\frac{\omega_j(q)}{2} t\right) \\ &\leq \int_0^{Q_B} dq q^2 \Gamma_j(q) [2 + 4n_j(q)]. \end{aligned} \quad (\text{A4})$$

The integral in Eq. (A4) exists and has a finite value, because the integration is over a finite range and the integrand is continuous with the exception of the point $q=0$ where it has an integrable singularity. The integrability of the singularity follows from the small q behavior of the functions $\Gamma_j(q)$, $n_j(q)$ and $\omega_j(q)$. More specifically, we find for small q : $\omega_j(q) \rightarrow \omega_{\text{LO}}$ for the optical branch and $\omega_j(q) \rightarrow c_j q$ for the acoustic branches, where c_j are the respective sound velocities. As already discussed in the text the couplings $g_{j,\mathbf{q}}^x := g_{j,\mathbf{q}}^e - g_{j,\mathbf{q}}^h$ scale as $q^{1/2}$ for deformation potential and as $q^{3/2}$ for piezoelectric coupling. For the Fröhlich coupling we obtain from Eq. (4) that the bulk couplings are equal for

electrons and holes and scale like $1/q$. As in the piezoelectric case accounting for the cancellation of the electron and hole form factors yields an extra factor q^2 such that $g_{\text{LO},\mathbf{q}}^x \sim q$. Thus for the asymptotics of $\Gamma_j(q) \sim |\gamma_j(\mathbf{q})|^2 = |g_{j,\mathbf{q}}^x / \omega_j(q)|^2$ we obtain $1/q$, q , and q^2 in the cases deformation potential, piezoelectric, and Fröhlich coupling, respectively. Finally, in the small q limit $n_j(q)$ approaches a finite constant for LO phonons, while for acoustic phonons we find $n_j(q) \rightarrow k_b T / (\hbar c_j q)$. The strongest singularity ($\sim 1/q^2$) therefore results from the deformation potential and is canceled by the factor q^2 from the volume element. Consequently, $F(t)$ is bounded by time-independent bounds and thus $|P|$ never approaches zero.

It is instructive to rewrite Eq. (A2) in the form $F(t) = t f(t)$. Then, by using the identity

$$\lim_{t \rightarrow \infty} \frac{\sin^2(xt)}{\pi t x^2} = \delta(x),$$

we find

$$\begin{aligned} \lim_{t \rightarrow \infty} f(t) &= \int_0^{Q_B} dq q^2 \Gamma_j(q) [2 \\ &+ 4n_j(q)] \pi \left(\frac{\omega_j(q)}{2}\right)^2 \delta\left(\frac{\omega_j(q)}{2}\right). \end{aligned} \quad (\text{A5})$$

The LO branch does not contribute to Eq. (A5), because $\omega_{\text{LO}}(q)$ has no zeros. For the acoustic branches the only zero is at $q=0$ and each branch contributes a part $\lim_{q \rightarrow 0^+} \pi c_j q^4 \Gamma_j(q) [1 + 2n_j(q)]$ which also vanishes due to the asymptotics discussed above. The interesting insight here is that the occurrence of the δ function in Eq. (A5) explicitly prove that the asymptotic behavior for large t is determined exclusively by the behavior of the couplings in the vicinity of $q=0$. This also sheds light on the previous finding by Duke and Mahan²⁰ that without the cancellation of electron and hole parts at small q values the zero phonon line acquires a finite width. While Duke and Mahan used model wave functions such that all q integrations could be performed analytically, it now becomes clear that the width of the zero-phonon line is determined only by the scaling of the phonon coupling in the limit $q \rightarrow 0$; in the case discussed in Ref. 20 this scaling was given by $\Gamma_j(q) \sim 1/q^3$. And indeed, using this small q behavior in Eq. (A5) we find that $f(t)$ in the limit $t \rightarrow \infty$ approaches a finite value indicating that $|P(t)|$ asymptotically exhibits an exponential decay towards zero. Obviously, the exponent given by the asymptotics of $f(t)$ also determines the width of the zero-phonon line.

¹D. Bimberg, M. Grundmann, and N. N. Ledentsov, *Quantum Dot Heterostructures* (John Wiley & Sons, Chichester, 1998).

²A. Barenco, D. Deutsch, A. Ekert, and R. Josza, Phys. Rev. Lett. **74**, 4083 (1995).

³P. Zanardi and F. Rossi, Phys. Rev. Lett. **81**, 4752 (1998).

⁴D. Loss and D.P. DiVincenzo, Phys. Rev. A **57**, 120 (1998).

⁵M.S. Sherwin, A. Imamoglu, and T. Montroy, Phys. Rev. A **60**, 3508 (1999).

⁶G. Burkard, D. Loss, and D.P. DiVincenzo, Phys. Rev. B **59**, 2070 (1999).

⁷T. Tanamoto, Phys. Rev. A **61**, 022305 (2000).

⁸E. Biolatti, R.C. Iotti, P. Zanardi, and F. Rossi, Phys. Rev. Lett.

- 85**, 5647 (2000).
- ⁹U. Bockelmann and G. Bastard, Phys. Rev. B **42**, 8947 (1990).
- ¹⁰H. Benisty, Phys. Rev. B **51**, 13 281 (1995).
- ¹¹S. Mukamel, *Principles of Nonlinear Optical Spectroscopy* (Oxford University Press, New York, 1995).
- ¹²T. Takagahara, Phys. Rev. B **60**, 2638 (1999).
- ¹³P. Palinginis and H. Wang, Appl. Phys. Lett. **78**, 1541 (2001).
- ¹⁴D. Gammon, E. S. Snow, B. V. Shanbrook, D. S. Katzer, and D. Park, Science **273**, 87 (1996).
- ¹⁵N.H. Bonadeo, C. Chen, D. Gammon, D.S. Katzer, D. Park, and D.G. Steel, Phys. Rev. Lett. **81**, 2759 (1998).
- ¹⁶A. Zrenner, J. Chem. Phys. **112**, 7790 (2000).
- ¹⁷P. Borri, W. Langbein, J.M. Mørk, J.M. Hwang, F. Heinrichsdorf, M.-H. Mao, and D. Bimberg, Phys. Rev. B **60**, 7784 (1999).
- ¹⁸P. Borri, W. Langbein, E. Schneider, U. Woggon, R.L. Sellin, D. Ouynag, and D. Bimberg, Phys. Rev. Lett. **87**, 157 401 (2001).
- ¹⁹K. Huang and A. Rhys, Proc. R. Soc. London, Ser. A **204**, 406 (1950).
- ²⁰C.B. Duke and G.D. Mahan, Phys. Rev. **139**, A1965 (1965).
- ²¹S. Schmitt-Rink, D.A.B. Miller, and D.S. Chemla, Phys. Rev. B **35**, 8113 (1987).
- ²²A.V. Uskov, A.-P. Jauho, B. Tromborg, J. Mørk, and R. Lang, Phys. Rev. Lett. **85**, 1516 (2000).
- ²³T. Takagahara, Phys. Rev. Lett. **71**, 3577 (1993).
- ²⁴R. Heitz, I. Makhmetzhanov, O. Stier, A. Madhukar, and D. Bimberg, Phys. Rev. Lett. **83**, 4654 (1999).
- ²⁵G. Mahan, *Many-Particle Physics* (Plenum, New York, 1990).
- ²⁶M.U. Wehner, M.H. Ulm, D.S. Chemla, and M. Wegener, Phys. Rev. Lett. **80**, 1992 (1998).
- ²⁷V.M. Axt, M. Herbst, and T. Kuhn, Superlattices Microstruct. **26**, 117 (1999).
- ²⁸D. Steinbach, G. Kocherscheidt, M. U. Wehner, H. Kalt, M. Wegener, K. Ohkawa, D. Hommel, and V. M. Axt, Phys. Rev. B **60**, 12 079 (1999).
- ²⁹H. Castella and R. Zimmermann, Phys. Rev. B **59**, R7801 (1999).
- ³⁰X. Fan, T. Takagahara, J.E. Cunningham, and H. Wang, Solid State Commun. **108**, 857 (1998).
- ³¹G. D. Mahan, in *Polarons in Ionic Crystals and Polar Semiconductors*, edited by J. T. Devreese (North-Holland, Amsterdam, 1972), p. 533.
- ³²V. M. Axt and S. Mukamel, in *Nonlinear Optical Materials*, IMA Volumes in Mathematics and Its Applications, edited by J. Maloney (Springer, Berlin, 1997), Vol. 101, p. 1.
- ³³J. Schilp, T. Kuhn, and G. Mahler, Phys. Rev. B **50**, 5435 (1994).
- ³⁴T. Kuhn, in *Theory of Transport Properties of Semiconductor Nanostructures*, edited by E. Schöll (Chapman and Hall, London, 1998), p. 173.
- ³⁵L. Jacak, P. Hawrylak, and A. Wójs, *Quantum Dots* (Springer, Berlin, 1998).
- ³⁶S. Adachi, *GaAs and Related Materials* (World Scientific, Singapore, 1994).
- ³⁷T. Kuhn, V. M. Axt, M. Herbst, and E. Binder, in *Coherent Control in Atoms, Molecules, and Semiconductors*, edited by W. Pötz and W. A. Schroeder (Kluwer Academic, Dordrecht, 1999), p. 113.
- ³⁸G. Scamarcio, V. Spagnolo, G. Ventruti, M. Lugará, and G.C. Righini, Phys. Rev. B **53**, R10 489 (1996).
- ³⁹R. Heitz, I. Makhmetzhanov, O. Stier, A. Madhukar, and D. Bimberg, Physica E (Amsterdam) **7**, 398 (2000).
- ⁴⁰G.W. Wen, J.Y. Lin, H.X. Jiang, and Z. Chen, Phys. Rev. B **52**, 5913 (1995).
- ⁴¹S.-S. Li and J.-B. Xia, J. Appl. Phys. **88**, 7171 (2000).
- ⁴²P.W. Fry, I.E. Itskevich, D.J. Mowbray, M.S. Skolnick, J.J. Finley, J.A. Barker, E.P. O'Reilly, L.R. Wilson, I.A. Larkin, P.A. Maksym, M. Hopkinson, M. Al-Khafaji, J.P.R. David, A.G. Cullis, G. Hill, and J.C. Clark, Phys. Rev. Lett. **84**, 733 (2000).
- ⁴³T.M. Hsu, W.-H. Chang, C.C. Huang, N.T. Yeh, and J.-I. Chyi, Appl. Phys. Lett. **78**, 1760 (2001).
- ⁴⁴A.D. Andreev and E.P. O'Reilly, Phys. Rev. B **62**, 15 851 (2000).
- ⁴⁵M. Grundmann, O. Stier, and D. Bimberg, Phys. Rev. B **52**, 11 969 (1995).
- ⁴⁶M.A. Cusack, P.R. Briddon, and M. Jaros, Phys. Rev. B **54**, R2300 (1996).
- ⁴⁷O. Stier, M. Grundmann, and D. Bimberg, Phys. Rev. B **59**, 5688 (1999).
- ⁴⁸*Physics of Group IV Elements and III-V Compounds*, edited by O. Madelung, Landolt Börnstein, New Series, Group III, Vol. 17, Pt. a (Springer, Berlin, 1982).